

Schwinger boson mean-field theory: Numerics for the energy landscape and gauge excitations in two-dimensional antiferromagnets

G. Misguich

Institut de Physique Théorique, CEA, IPhT, CNRS, URA 2306, F-91191 Gif-sur-Yvette, France

(Received 20 August 2012; revised manuscript received 29 November 2012; published 27 December 2012)

We perform some systematic numerical search for Schwinger boson mean-field states on square and triangular clusters. We look for possible inhomogeneous ground states as well as low-energy excited saddle points. The spectrum of the Hessian is also computed for each solution. On the square lattice, we find gapless $U(1)$ gauge modes in the nonmagnetic phase. In the \mathbb{Z}_2 liquid phase of the triangular lattice, we identify the topological degeneracy as well as vison states.

DOI: [10.1103/PhysRevB.86.245132](https://doi.org/10.1103/PhysRevB.86.245132)

PACS number(s): 75.10.Jm, 75.50.Ee, 71.10.Hf

I. INTRODUCTION

Quantum antiferromagnets can display complex many-body phenomena, with rich phase diagrams, exotic states of matter with emerging degrees of freedom.¹ Indeed, minimizing a rather simple looking interaction like the Heisenberg one, $\vec{S}_i \cdot \vec{S}_j$, can lead to a vast variety of states of matter, depending on the size $\vec{S}_i^2 = S(S+1)$ of the spins, the space dimension, geometry of the lattice, or relative strengths of possible competing interactions (frustration, etc.). In fact, after many years of theoretical investigations, the nature of the ground state of the spin-1/2 Heisenberg model remains controversial on several two- and three-dimensional lattices. Some of the most interesting states that can be stabilized at $T = 0$ are called *spin liquids* and have no direct classical analogs. These systems remain rotationally invariant down to zero temperature. There is a whole zoo of possible spin liquids, and the most exotic one have low-energy excitations that carry a half-odd-integer spin (unlike conventional spin waves).

There are rather few theoretical tools that are able to describe the limit of strong quantum fluctuations (small S) for these systems, and spin liquid phases in particular. Among them, the so-called large- N techniques, introduced by Affleck for spin chains,² play a central role. By generalizing the symmetry group of global spin rotations from $SU(2)$ to some larger group like $SU(N)$ or $Sp(2N)$,³ the model can be solved in the limit $N = \infty$. Of course, the physics for $N = 2$ needs not be simply related to that at $N = \infty$. However, the success of these approaches is in part due to the fact that a number of interesting states that can be realized for $SU(2)$ models, also exist in the $N = \infty$ phase diagrams. In particular, the $N = \infty$ models are not restricted to have magnetically ordered ground state, and can have resonating valence-bond spin liquids ground states with fractionalized excitations and emerging gauge degrees of freedom. Furthermore, the effect of finite- N corrections (both perturbative^{4,5} and nonperturbative ones⁶) can be addressed.

In this work, we consider a particular large- N limit, the so-called Schwinger boson mean-field theory (SBMFT).^{3,7} It has been applied to many two-dimensional systems, such as the $J_1 - J_2$ square,⁸ triangular,⁹⁻¹² honeycomb,^{13,14} kagome,^{9,15-17} kagome with further neighbor interactions,^{17,18} Shastry-Sutherland,^{19,20} or CaV_4O_9 ²¹ lattices. This limit can in particular stabilize magnetically ordered (Néel) states as well as \mathbb{Z}_2 spin liquids with gapped spinons.⁹

The model contains N flavors of spin-1/2 bosons (spinons) and the parameter that plays the role of the spin value $2S$ is the number κ of bosons per site (and per flavor). After performing a Hubbard-Stratonovich decoupling of the boson-boson interaction, the different boson flavors are coupled to a single complex field A_{ij} on each bond ij of the lattice. The formal (Gaussian) integration of the spinons gives an effective action $S_{\text{eff},N}[A]$ for the bond field. But the dependence in N is simple since this action is that of the single-flavor problem multiplied by a factor N : $S_{\text{eff},N}[A] = N S_{\text{eff},1}[A]$. When N is large, it is therefore natural to perform a saddle point expansion. At the saddle point, the bond-field fluctuations are frozen, and the effective Hamiltonian is simply quadratic in the spinon operators. So the action can be computed with the help of a standard Bogoliubov transformation. Finding a large- N ground state thus amounts to solving a classical minimization problem.

Previous SBMFT studies have mostly been focused on the ground-state properties at $N = \infty$. However, as a first step to understand the effects of finite- N corrections, it is interesting to have access to the low-energy energy landscape of saddle points. Although the system is locked into the lowest one when $N = \infty$, the (large but) finite- N physics must include some fluctuations between different low-energy saddle points, as well as some (perturbative in $1/N$) fluctuations in the vicinity of each of these saddle points. Our goal here is to provide a quantitative description of some excited saddle points.

In order to reduce the number of variables, it is almost always assumed that the lowest-energy state preserves most (or at least some) of the lattice symmetries (see Ref. 22 for a notable exception). In practice, most numerical studies have so far been restricted to solutions with a unit cell including a few sites only. This is a reasonable assumption for the ground state, and we confirm its validity in several cases. However, since we are interested here in excited saddle points, we need to be able to compute some *spatially inhomogeneous* states as well. We will, however, limit ourselves to time-independent solutions.

In this work, we perform some extensive numerical minimization to look for the ground state and low-energy excited states on clusters containing up to 144 sites. We compare the results we obtain on two different lattices (square and triangular) and for different values of the boson density ("spin") κ .

II. SCHWINGER BOSON MEAN-FIELD THEORY

To keep this article self-contained, this section presents the basic ideas and notations of the SBMFT (see also Refs. 23 and 24). “Up” and “down” bosons operators ($\sigma \in \{\uparrow, \downarrow\}$), carrying a spin $S = 1/2$, are introduced at each lattice site: $b_{i\sigma}^\dagger$ and $b_{i\sigma}$. The spin operators can then be written:

$$S_i^+ = b_{i\uparrow}^\dagger b_{i\downarrow}, \quad (1)$$

$$S_i^- = b_{i\downarrow}^\dagger b_{i\uparrow}, \quad (2)$$

$$2S_i^z = b_{i\uparrow}^\dagger b_{i\uparrow} - b_{i\downarrow}^\dagger b_{i\downarrow}. \quad (3)$$

These relations imply that the commutation relations $[S_i^\alpha, S_i^\beta] = i\epsilon^{\alpha\beta\delta} S_i^\delta$ are automatically verified. The total spin reads $\vec{S}_i^2 = \frac{n_i}{2}(\frac{n_i}{2} + 1)$, where $n_i = b_{i\uparrow}^\dagger b_{i\uparrow} + b_{i\downarrow}^\dagger b_{i\downarrow}$ is the total number of bosons at site i . To fix the “length” of the spins, the following constraint must therefore be imposed on physical states:

$$\forall i, \quad \sum_{\sigma} b_{i\sigma}^\dagger b_{i\sigma} = \kappa = 2S. \quad (4)$$

The Heisenberg exchange Hamiltonian is biquadratic in the b operators and reads

$$H = \sum_{\langle ij \rangle} J_{ij} \mathbf{S}_i \cdot \mathbf{S}_j \quad (5)$$

$$= \frac{1}{4} \sum_{\langle ij \rangle} J_{ij} (b_{i\sigma}^\dagger \vec{\sigma}_{\sigma, \sigma'} b_{i\sigma'}) \cdot (b_{j\tau}^\dagger \vec{\sigma}_{\tau, \tau'} b_{j\tau'}), \quad (6)$$

where $\vec{\sigma}$ is the vector whose components are the Pauli matrices, and each lattice bond ij is taken only once. It is convenient to rewrite H using rotationally invariant bond operators:

$$H = \sum_{\langle ij \rangle} J_{ij} (: \hat{B}_{ij}^\dagger \hat{B}_{ij} : - \hat{A}_{ij}^\dagger \hat{A}_{ij}), \quad (7)$$

where $: - :$ represents normal ordering and the bond operators \hat{A}_{ij} and \hat{B}_{ij} are

$$\hat{A}_{ij} = \frac{1}{2}(b_{i\uparrow} b_{j\downarrow} - b_{i\downarrow} b_{j\uparrow}), \quad (8)$$

$$\hat{B}_{ij} = \frac{1}{2}(b_{i\uparrow}^\dagger b_{j\uparrow} + b_{i\downarrow}^\dagger b_{j\downarrow}). \quad (9)$$

\hat{A}_{ij}^\dagger creates a spin singlet on the (oriented) bond ij whereas \hat{B}_{ij}^\dagger creates a triplet. Due to the constraints, these operators are linked by the relation

$$: \hat{B}_{ij}^\dagger \hat{B}_{ij} : + \hat{A}_{ij}^\dagger \hat{A}_{ij} = S^2 \quad (10)$$

and it is therefore possible to express the Hamiltonian using \hat{A} only:

$$H = \sum_{\langle ij \rangle} J_{ij} (S^2 - 2\hat{A}_{ij}^\dagger \hat{A}_{ij}). \quad (11)$$

The SB mean-field approximation—which can be formally justified in a large- N limit of the model—consists in decoupling the quartic terms and to add some chemical potentials λ_i to tune the *average* number of boson at each site [instead of

Eq. (4)]. The resulting mean-field Hamiltonian is

$$H_{\text{MF}} = \sum_{\langle ij \rangle} J_{ij} (S^2 - 2\bar{A}_{ij} \hat{A}_{ij} - 2A_{ij} \hat{A}_{ij}^\dagger + 2|A_{ij}^2|) - \sum_i \lambda_i (b_{i\sigma}^\dagger b_{i\sigma} - \kappa), \quad (12)$$

where \bar{x} is the conjugate of x , A_{ij} are complex link variables with property $A_{ij} = -A_{ji}$. It is also possible to write a mean-field theory keeping simultaneously both operators \hat{A} and \hat{B} on each bond.^{25,26} This will, however, not be considered here.²⁷

It is convenient to write H_{MF} by grouping the creation and annihilation operators in a vector $\hat{\phi} = (b_{1\uparrow}, \dots, b_{N_S\uparrow}, b_{1\downarrow}, \dots, b_{N_S\downarrow})^t$, where N_S is the number of sites in the lattice. Eq. (12) then reads

$$H_{\text{MF}} = (\hat{\phi})^\dagger M \hat{\phi} + \text{const}, \quad (13)$$

where M is a $2N_S \times 2N_S$ matrix:

$$M = \begin{bmatrix} -\lambda_i & J_{ij} A_{ij} \\ -J_{ij} \bar{A}_{ij} & -\lambda_i \end{bmatrix}. \quad (14)$$

For simplicity, we restrict the discussion to finite systems where H_{MF} has a gapped spectrum (possibly vanishing in the thermodynamic limit). The ground state exists and its spectrum is gapped if and only if the the matrix M is positive definite.²⁸

We define a diagonal $2N_S \times 2N_S$ matrix σ : $\sigma = \begin{bmatrix} -1 & 0 \\ 0 & 1 \end{bmatrix}$ and, with the gap condition, σM is diagonalizable (although not Hermitian) and has pairs of real eigenvalues $\pm\omega_n = 1, \dots, N_S$, where the $\omega_n > 0$ are the of the Bogoliubov modes of H_{MF} . The ground-state energy of H_{MF} is given by

$$E_{\text{MF}} = \sum_n \omega_n + \sum_{ij} J_{ij} |A_{ij}|^2 + (2S + 1) \sum_i \lambda_i \quad (15)$$

(remark: in a large- N formalism, this corresponds to the energy *per flavor*).

The self consistency is reached when $A_{ij} = \langle \hat{A}_{ij} \rangle_{GS}$, which is equivalent to $\partial E / \partial A_{ij} = 0$, where E is the energy of the ground state of H_{MF} . The average number of boson per site is equal to $2S$ [see Eq. (4)] at the point(s) where $\partial E / \partial \lambda_i = 0$. Since $\partial^2 E / \partial \lambda^2 \leq 0$ (see this footnote²⁹), this point corresponds to a *maximum* of $\{\lambda_i\} \mapsto E[\{A_{ij}\}, \{\lambda_i\}]$. For fixed $\{A_{ij}\}$, this allows to use a maximization algorithm to determine the chemical potentials $\lambda_i[\{A_{ij}\}]$. In a similar way, the self-consistent $\{A_{ij}\}$ correspond to a *minimum* of $E[\{A_{ij}\}, \lambda_i[\{A_{ij}\}]]$ if the J_{ij} are positive.

A. Gauge invariance and fluxes

The solution of this system of equations is not unique, at least because of the $U(1)$ gauge invariance of the Hamiltonian. Under the gauge transformation

$$b_{j\sigma} \rightarrow e^{i\theta(j)} b_{j\sigma}, \quad \hat{A}_{ij} \rightarrow e^{i(\theta(i)+\theta(j))} \hat{A}_{ij}, \quad (16)$$

the physical operators (as \vec{S}_i or H) stay unchanged. In other words, the bond parameters A_{ij} label the physical state in a redundant way. Using gauge transformations, we can fix the phases of some A_{ij} , without changing any physical observable.

This decreases the number of variables to be optimized and is, therefore, useful in numerical studies.

The moduli $|A_{ij}|$ are of course gauge invariant quantities, simply related to the energy. But some combinations of complex phases around closed loops are also gauge invariant. Consider the following operator $\hat{\mathbb{A}}_{i_1 i_2 \dots i_{2n}}$

$$\hat{\mathbb{A}}_{i_1 i_2 \dots i_{2n}} = \hat{\mathbb{A}}_{i_1 i_2} (-\hat{\mathbb{A}}_{i_2 i_3}^\dagger) \hat{\mathbb{A}}_{i_3 i_4} \dots (-\hat{\mathbb{A}}_{i_{2n} i_1}^\dagger). \quad (17)$$

This operator is defined on any loop with an even length on the lattice and is manifestly gauge invariant. Its mean-field (or large- N) counter part,

$$\mathbb{A}_{i_1 i_2 \dots i_{2n}} = A_{i_1 i_2} (-\bar{A}_{i_2 i_3}) A_{i_3 i_4} \dots (-\bar{A}_{i_{2n} i_1}), \quad (18)$$

gives the flux $\phi_{i_1 i_2 \dots i_{2n}} = \arg(\mathbb{A}_{i_1 i_2 \dots i_{2n}})$ recently discussed by Tchernyshyov *et al.*³⁰

In general, the number of variables (all the moduli, plus some phases) grows with the system size. Since it is quite difficult to perform an exhaustive search for mean-field solutions if the number of parameters is extensive, the usual strategy is to decrease the number of bond variables by *assuming* that the ground-state solution preserves some (or all) symmetries of the lattice. There are, however, some examples where the lowest energy solution spontaneously *breaks* some symmetries (kagome clusters with 36 or 48 sites³¹).

III. NUMERICAL METHOD

We describe an algorithm to find saddle points (self-consistent mean-field state), local minima, and (hopefully) global energy minima.

A. Determination of the chemical potentials

For given values of the bond parameters A_{ij} , one should first adjust the chemical potentials $\{\lambda_i\}$. The basic idea is to perform a (nonlinear) least-square minimization of $\sum_i f_i^2$, where $f_i(\{\lambda_j\}) = \langle \hat{n}_i \rangle - \kappa$ is a function of the chemical potentials. Since each density $\langle \hat{n}_i \rangle$ is an increasing function of λ_i , this method converges relatively rapidly. To do so, we use an implementation of the Levenberg-Marquart algorithm.³² To make the method faster, we provide the gradient matrix $G_{ij} = \frac{\partial \langle \hat{n}_i \rangle}{\partial \lambda_j}$ explicitly. G_{ij} is easy to compute using linear-response theory (using the matrix which implements the Bogoliubov transformation, as well as the energies ω_i). The iterative minimization should start in a region of the space of λ where the Bogoliubov transformation exist ($M > 0$). If the values of λ obtained at the previous step do not satisfy this condition with the new $\{A_{ij}\}$, one starts the least-square minimization of $\sum_i f_i^2$ from a sufficiently low and uniform λ .

Finally, we note that for some values of the bond parameters A_{ij} , there is no uncondensed state satisfying $\langle \hat{n}_i \rangle = \kappa$. If such a situation is encountered, we add some artificial energy penalty so that the energy-minimization algorithm (next section) tends to escape this point.

B. Optimization of the bond parameters A_{ij}

Equipped with a procedure to compute the λ_i as a function of the A_{ij} , we can start to look values of A_{ij} which correspond to self-consistent mean-field states. The first stage is simply to iterate the bond self-consistency conditions in the usual way: (1) we start from initial random bond values (or

perturbing a previously found solution). (2) After adjusting the λ by the procedure above, the ground state is obtained by Bogoliubov transformation, and the expectation values $\langle A_{ij} \rangle$ are computed. (3) The bond parameters are replaced by the values above. The new bond parameters are gauge transformed to a fixed gauge choice where a maximum number of bond parameters are set to be real. This avoids some possible slow drift of some complex phases of the A_{ij} which would be nonphysical. (4) Go back to step 2 until the bond parameters do not change by more than a small threshold ϵ .

This method was used by Hermele *et al.*²² in a similar context. It is easy to check that local minima are attractive for these iterations while local maxima a repulsive. More precisely, the error will decrease (respectively increase) in the directions corresponding to eigenvectors of the Hessian [anticipating on Eq. (20)] with positive (respectively negative) values. The convergence is faster if the Hessian eigenvalues are large and positive. In practice, the iterations above allow to quickly go down in energy, but it is not efficient to achieve a full convergence when the system has more than ~ 10 bonds or so. Indeed, it turns out that a high accuracy is required to resolve the possibly small differences (bond modulations, etc.) between different saddle points.

To find accurately the self-consistent state, the second stage amounts to perform a least-square optimization on $\sum_{ij} g_{ij}^2$, where $g_{ij}(\{A\}) = \langle \hat{A}_{ij} \rangle - A_{ij}$ is a function of the bond parameters. Of course, the expectation values $\langle \hat{A}_{ij} \rangle$ are computed after the $\lambda_i(\{A\})$ have been determined. This second stage allows to converge not only to local extrema but to saddle points as well. Again, we use a Levenberg-Marquart minimization algorithm,³² with explicit calculation of the gradient $\frac{\partial \langle \hat{A}_{ij} \rangle}{\partial A_{kl}}$ at fixed densities $\langle \hat{n} \rangle = \kappa$. The later is again obtained using linear-response theory, with the additional complexity that it contains some terms coming from the variation of the λ :

$$\begin{aligned} \frac{\partial \langle \hat{A}_{ij} \rangle}{\partial A_{kl}} \Big|_{\langle \hat{n} \rangle = \kappa} &= \frac{\partial \langle \hat{A}_{ij} \rangle}{\partial A_{kl}} \Big|_{\lambda \text{ fixed}} + \sum_{a,b} \frac{\partial \langle \hat{A}_{ij} \rangle}{\partial \lambda_a} \\ &\times \left[\frac{\partial \langle \hat{n} \rangle}{\partial \lambda} \right]_{ab}^{-1} \frac{\partial \langle \hat{n}_b \rangle}{\partial A_{kl}} \Big|_{\lambda \text{ fixed}}. \end{aligned} \quad (19)$$

As for the first stage, we work with bond variables corresponding to a fixed gauge choice. In particular, the matrix of Eq. (19) is evaluated in the subspace of bond parameter variations that are orthogonal to pure gauge transformations. This is important to get rid of unphysical slow phase drifts during the iterations. Most of the time a double precision accuracy is reached in less than ten Levenberg-Marquart iterations when the system has less than one hundred bonds or so.

Finally, the optimization is repeated using at least a few hundred (often thousands) of random initial conditions for the A_{ij} . This is relatively time consuming since each evaluation of the energy (or its derivatives) requires a numerical adjustment of the chemical potentials (see Sec. III A), which is itself a (convex) least-square problem with many variables.

Varying the parameter ϵ (stopping criterion for the iterations of stage 1) allows to tune if the method will converge toward very low-energy saddle points (small ϵ), or saddle point at higher energy (larger ϵ). If ϵ is very small (say 10^{-5}), the first

stage will terminate close to the ground state and the second step (least-square) will converge to the ground state with high probability if the system is not too large ($\lesssim 100$ bonds). On the other hand, if ϵ is too large, the first stage will stop at some relatively high energy configuration. In such region of the A space, we expect a very (exponentially) high density of saddle points. In practice, this density of saddle point is so high that the program will find a new solution at every run, and a given saddle point will rarely be obtained twice. The best choice is to adjust ϵ so that the iteration stage leads to configurations in a typical energy range above the ground state where the number of saddle points is not too large (a few tens). In such a case, after a sufficiently large number of runs, one obtains the full (or almost full) list of saddle points in that energy window. Of course, due to the large number of variables, one cannot exclude the presence of some additional saddle points with a small basin of attraction with respect to this algorithm.

C. Hessian and stability

The least-square procedure described above leads to self-consistent mean-field states, satisfying $A_{ij} = \langle \hat{A}_{ij} \rangle$. These states are saddle point of the energy (considered as a function of the A_{ij} , and the chemical potential being themselves functions of the A_{ij}). To check if each mean-field state is a local minimum, local maximum, or generic saddle points with stable as well as unstable directions, we compute the Hessian matrix:

$$K_{l,l'} = \frac{\partial^2 E_{\text{MF}}}{\partial A_l^\epsilon \partial A_{l'}^{\epsilon'}} = 4J_l \left(\delta_{ll'} \delta_{\epsilon\epsilon'} - \frac{\partial \langle \hat{A}_l^\epsilon \rangle}{\partial A_{l'}^{\epsilon'}} \Big|_{\langle \hat{n}_i \rangle = \kappa} \right), \quad (20)$$

where l and l' represent two bonds and ϵ and ϵ' denote the real or imaginary part of the bond variables [see Eq. (19) for derivatives of the bond expectation values at fixed densities].

Due to the gauge invariance of the model, the Hessian contains some zero eigenvalues associated to infinitesimal gauge transformations. The number of such gauge modes can be computed on each given lattice (using the rank of a modified adjacency matrix of the lattice³³), and these nonphysical zero eigenvalues are of course discarded when discussing these solutions. For the clusters studied here, the number of zero eigenvalues is always equal to the number of pure gauge modes, so we can conclude that there is no *physical* zero mode in the Hessian. The sign of the smallest nonzero eigenvalue of K tells us whether the mean-field state is a local minimum, or an unstable saddle point.

The spectrum of the Hessian for the ground state gives some information about the magnitude of the $1/N$ corrections due to Gaussian fluctuations in the vicinity of the energy minimum. Finally, the spatial structure of the lowest eigenvector of the Hessian gives some information about the physical nature of these fluctuations.

IV. NUMERICAL RESULTS

A. Square lattice

The SBMFT phase diagram is well known on the square lattice: magnetic long-range order for $\kappa \gtrsim 0.39$ (see Ref. 7) and a disordered phase with gapped spinons for $\kappa \lesssim 0.39$ [“Coulomb” phase, unstable at finite- N (see Ref. 6)]. In the ordered phase, the spinon gap drops as $\sim 1/N_s$ (N_s is the

number of sites) and Bose-condensation occurs in the thermodynamic limit, leading to spontaneous break down of the spin rotation symmetry. By considering here only finite clusters, the ground state is always rotationally invariant and the gap finite. Still, both phases can be distinguished using standard finite size-scaling for the gap or spin-spin correlations. We will discuss how the “energy landscape” of mean-field saddle points differ between the two phases.

1. Hessian of the ground state and gauge modes

We did some extensive search for saddle points on square lattices with 36 sites and with $\kappa = 0.1$ and $\kappa = 1$. The ground state, as expected, is spatially uniform, real, and has a vanishing flux on all the square plaquettes, whatever the boson density. However, the spectrum of the Hessian is quite different in the magnetic phase and in the disordered phase.

In Fig. 1, the smallest eigenvalue of the Hessian [see Eq. (20)] is plotted as a function of the κ for different system sizes (up to 144 sites). Although finite-size effects are important, these data indicate that the Hessian is gapped in the thermodynamic limit for large κ , while it becomes gapless for small κ . The transition very likely coincides with that of magnetic long-range order.

The gaplessness of the Hessian in the disordered region is due to the bipartite character of the lattice. On a bipartite lattice, the bond parameters are invariant under *staggered* gauge transformations:

$$b_{r\sigma} \longrightarrow b_{r\sigma} e^{i(-1)^r \theta}, \quad (21)$$

$$A_{rr'} \longrightarrow A_{rr'}, \quad (22)$$

which, in Wen’s terminology,³⁴ means that the invariant gauge group (IGG) is $U(1)$.

If we perform a spatially varying gauge transformation including the staggered factor, we get

$$b_{r\sigma} \longrightarrow b_{r\sigma} e^{i(-1)^r \theta(r)}, \quad (23)$$

$$A_{rr'} \longrightarrow A_{rr'} e^{i[\theta(r) - \theta(r')]}, \quad (24)$$

where r (respectively, r') is on the even (respectively, odd) sublattice. Starting from a state described by $A_{rr'}^0$, we construct a phase fluctuation of the bond parameters parameterized by $a_{rr'} \in \mathbb{R}$:

$$A'_{rr'} = A_{rr'}^0 + dA_{rr'} = A_{rr'}^0 e^{ia_{rr'}}. \quad (25)$$

From Eq. (24), $a_{rr'}$ transforms as a conventional $U(1)$ gauge field:

$$a_{rr'} \longrightarrow a_{rr'} + \theta(r) - \theta(r'). \quad (26)$$

So, if we denote by $E(\{a_{rr'}\})$ the energy of the perturbed mean-field state (after the appropriate adjustment of the chemical potentials), the energy should be gauge invariant under Eq. (26). In the small- κ phase where the bosons are gapped and their correlation length is short, $E(\{a_{rr'}\})$ should be a local (short-ranged) function of the fluctuation $a_{rr'}$.

The simplest local term compatible with gauge invariance would be the lattice version of the magnetic energy $(\vec{\nabla} \times \vec{a})^2$, and would take the form of the square of the circulation of \vec{a} around small loops (this can also be obtained from a small- κ expansion³⁰). This would give an Hessian eigenvalue

scaling as the square of the smallest available wave vector, that is $\sim 1/L^2 \sim 1/N_s$ (L the linear size and N_s the number of sites). Such modes are indeed found in the spectrum of the

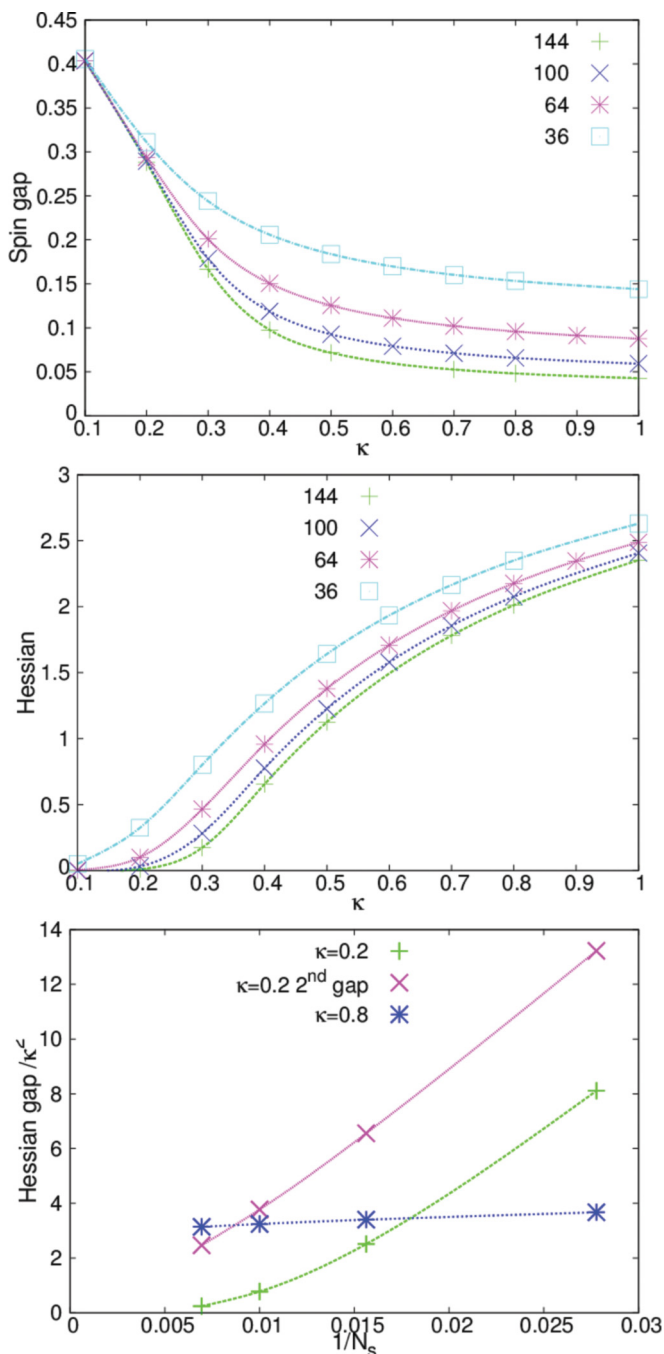


FIG. 1. (Color online) Square lattice model. (Top) Spin gap as a function of κ . In the thermodynamic limit this state is associated to magnetic long-range order (vanishing spin gap) for $\kappa > \kappa_c \simeq 0.39$.⁷ (Middle) Smallest eigenvalue of the Hessian for the ground state on 36, 64, and 144-site square lattices. (Bottom) Scaling of the lowest Hessian eigenvalue as a function of the system size N_s . This shows that the Hessian is gapless for $\kappa = 0.2$ and gapped for $\kappa = 0.8$. The Hessian gap is finite in the magnetic phase, while it vanishes in the thermodynamic limit for $\kappa < \kappa_c$. For $\kappa = 0.2$, first eigenvalues decays faster than $1/N_s$ whereas the second eigenvalue goes to zero as $\sim 1/N_s$ (see text).

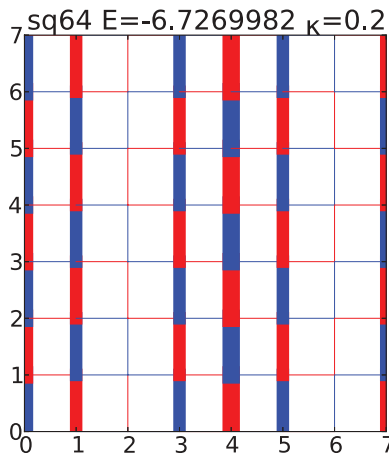


FIG. 2. (Color online) Hessian eigenvector dA_l corresponding to the second smallest eigenvalue (0.26224396339) for a 64-site square lattice with $\kappa = 0.2$. The thickness of each bond l is proportional to the modulus $|dA_l|$ while the color represents the complex argument of dA_l/A_l . Red: argument is $+\pi/2$, blue is $-\pi/2$. Here, dA is a gauge excitation, it corresponds to a long wavelength modulation of the flux through each plaquette. Here, the wave vector is parallel to the horizontal bonds. This gauge mode is associated to the smallest nonzero wave vector on the square lattice and is therefore fourfold degenerate.

Hessian and correspond to the *second* nonzero eigenvalue. The associated eigenvector is displayed in Fig. 2. The thickness of each bond l is related to the modulus $|dA_l|$ while the color represents the complex argument of dA_l/A_l . In the present case, these complex arguments take only two values: $\pm\pi/2$ (blue and yellow), indicating that dA is a *gauge mode* of the form of Eq. (25), with $dA_l/A_l^0 \sim ia_l \in i\mathbb{R}$. In the present case, $a_l \sim \cos(2\pi x_l/L)$ for a vertical link l (oriented from the even to the odd sublattice) at horizontal position x_l , and $a_l = 0$ on horizontal bonds. This gauge mode may be viewed as a low-energy “photon” of the effective gauge theory.⁶

In fact the numerical data indicate that the *lowest* eigenvalue of the Hessian decays *faster* than $1/N_s$ (see Fig. 1). The associated mode is represented in Fig. 3 and is also a gauge mode (dA_l/A_l^0 is purely imaginary). Inspecting the sign of a_l , one sees that it corresponds to a change in the “global” flux associated to the large loops encircling the torus while local loops are unaffected by this gauge mode. The structure of this eigenvector of the Hessian turns out to be the same for all system sizes we studied. We expect its eigenvalue to decay exponentially with the system size in the small- κ phase.

In the Néel phase, $E(\{a_{rr'}\})$ need not be short-ranged and the argument above fails. Indeed, the spinons are charged particles for the gauge field and their condensation gaps out the gauge degrees of freedom (Anderson-Higgs mechanism). In the Néel phase, computing the boson energy in presence of a global flux (through loops encircling the torus) amounts to impose some twist on the spin directions and the finite spin stiffness ρ naturally leads to an energy cost proportional to the square of the flux, and leads to a finite Hessian eigenvalue proportional to ρ . In turn, the finite Hessian gap in the Néel phase indicates a relative stability of the mean-field state with respect to Gaussian $1/N$ corrections.

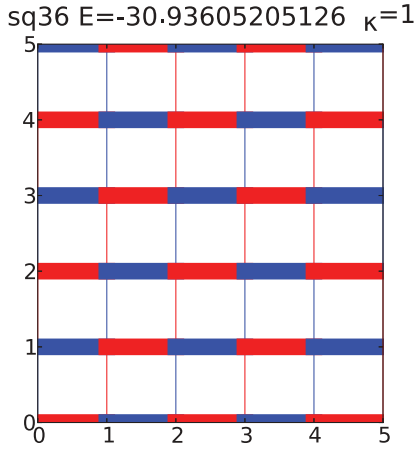


FIG. 3. (Color online) Hessian eigenvector dA_i corresponding to the smallest eigenvalue (2.62955994344) for a 36-site square lattice. Same representation as in Fig. 2. The complex argument of dA_i/A_i takes only two values: $\pm\pi/2$ (blue and red), indicating that dA is a gauge excitation. This mode corresponds to an increase of the flux through large horizontal loops, and no change for the flux going through local plaquettes.

2. Excited mean-field solutions for $\kappa = 1$

For $\kappa = 1$ (Néel phase), our search for saddle point on the 36 site cluster shows that the ground state (-30.93605205126) is well separated from the first excited saddle point ($E = -28.82425530821$, Fig. 4). No local minimum was found at low energy (see Table I), but only saddle points. In addition, the excited saddle points turn out to have very unstable directions (strongly negative Hessian eigenvalues). There might be some other mean-field states in the energy range of Table I, but these should have rather small basin of attraction with respect to our search algorithm, since this list of the twelve lowest energy state is stable after thousands of runs starting from random initial conditions.

The first excited saddle point is displayed in Fig. 4. It takes the form of an excitation localized around one site (here site number 14). This state is chiral, with a flux equal to $\pm 0.40461332\pi$ on the four square plaquettes touching the center of the excitation. The flux then decreases quickly with

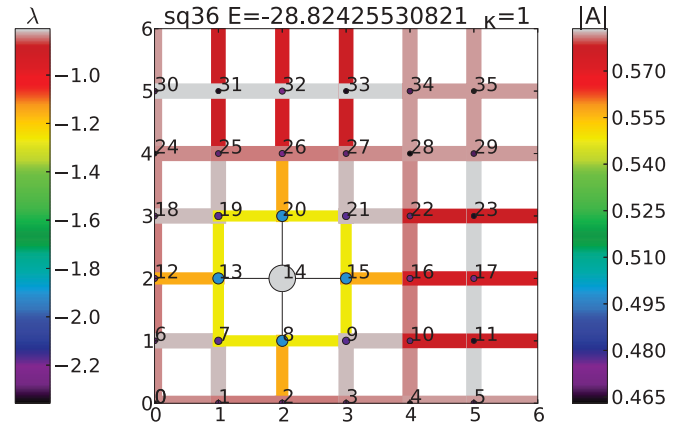


FIG. 4. (Color online) First excited mean-field solution on a square lattice with 36 sites and $\kappa = 1$. The modulus of the bond parameter (right color scale) is indicated, as well as the chemical potentials (left scale). This solution shows a localized excitation (here around site number 14). The flux decays rapidly with distance from the center: 0.4046133π on plaquette⁸, 9,15,¹⁴, 0.037028π on plaquette [1,2,8,7], -0.005291300π on [0,1,7,6], 0.0001131π on [4,5,11,10], etc. See Fig. 5 for some the spin-spin correlations in this state.

distance (see caption of Fig. 4), but the fact that some nontrivial fluxes (different from 0 or π) exist around the center of the excitation shows that it induces some nonplanar spin-spin correlations. Far from the center of the excitation, the spins remain in a collinear and in an ordered structure, as can be seen on the spin-spin correlations displayed in the bottom panel of Fig. 5. As for the center spin (number 14), it is correlated with its neighbors, but it is very weakly correlated ($\langle \vec{S}_{14} \cdot \vec{S}_i \rangle \simeq 0$) with the sites which are far apart (top of Fig. 5). Although the system is magnetically ordered, this pointlike “defect” does not seem do have a simple semiclassical analog. Interestingly, a similar pointlike “defect” excitation is found in the ordered phase of the triangular lattice.

3. Excited mean-field solutions for $\kappa = 0.1$

For $\kappa = 0.1$, the ground state on the square lattice is still uniform and without any flux, but the spinon gap (see Fig. 1)

TABLE I. Low-energy saddle points for a square lattice cluster with 36 sites and $\kappa = 1$. From the left column to the right: energy, spinon gap, lowest nonzero Hessian eigenvalue, degeneracy, number of different chemical potentials λ (1 means uniform, etc.), minimum and maximum values of λ , number of different values of $|A|$ minimum and maximum values of $|A|$, and real (R) or complex/chiral solution (C). The spatial modulations of $|A_{ij}|$ and λ_i for solution a are displayed in Fig. 4. Solution b has the same spatial structure (twofold degeneracy) as the one shown in Fig. 6(b).

E	Δ	H	d	N_λ	\min_λ	\max_λ	$N_{ A }$	$\min_{ A }$	$\max_{ A }$	
-30.93605205126	0.14402872021	2.6295599434	1	1	-2.33625413623	-2.33625413623	1	0.58295256650	0.58295256650	R
-28.82425530821 ^a	0.12128968489	-7.7009935434	36	10	-2.35767326534	-0.80802876988	12	0.46297459737	0.58363641125	C
-28.78219048843	0.10001664198	-50.5062824348	72	13	-2.36085237706	-0.70467719552	18	0.45635222273	0.59393955633	R
-28.36943538503	0.15018056150	-26.9056949522	72	12	-2.37180295956	-1.25427516482	25	3.06482822239e-15	0.78318014761	C
-27.87811171341	0.10635799592	-48.4908669283	72	12	-2.37611640988	-1.20158916706	18	0.33406678717	0.62744479349	R
-27.674044431445 ^b	0.24030790672	-33.3227937772	2	1	-2.12079971339	-2.12079971339	2	0.52769740399	0.59657118301	R
-27.58542591653	0.12018732985	-11.9733712946	72	16	-2.38843405218	-1.28794576300	24	0.29836817056	0.63116481780	C
-27.55178404956	0.08439099361	-67.0253600361	72	16	-2.48677863782	-1.13200578463	24	3.38069859599e-16	0.64685457030	C
-27.52461818853	0.19788831856	-3.8580290414	36	6	-2.23233357411	-1.87795360324	14	0.45547996236	0.59859663572	C
-27.49457258263	0.18888774623	-1.9063958450	36	8	-2.24866064506	-1.74743986196	14	0.46141122781	0.60087012841	C
-27.49456554040	0.19367584933	-5.7251545034	36	6	-2.22476689000	-1.75751056646	14	0.34656259228	0.60092322028	C
-27.40385237877	0.16760744308	-21.1217748777	144	18	-2.32248736876	-1.30042949863	38	0.27024089067	0.64068344661	C

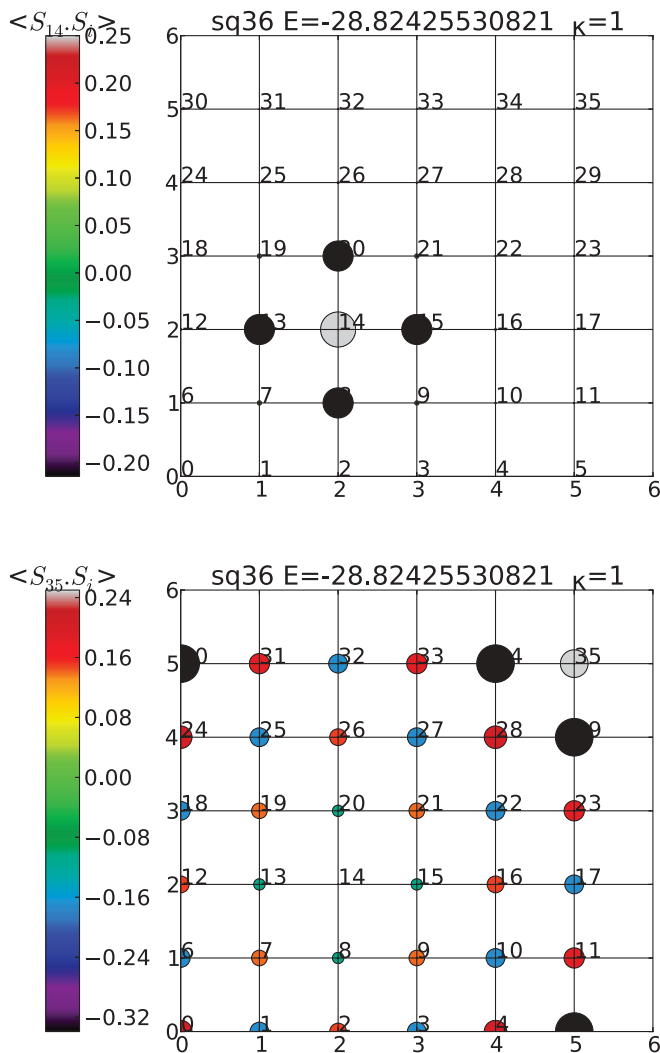


FIG. 5. (Color online) Spin-Spin correlation in the first excited of a 36-site square lattice with $\kappa = 1$ (same state as in Fig. 4). The radius of the circle on site j proportional to the correlation $|\langle \tilde{S}_{i_0} \tilde{S}_j \rangle|$ with the reference site i_0 (the sign is available on the color scale). (Top) Reference spin $i_0 = 14$ is at the center of the localized excitation. (Bottom) Reference spin $i_0 = 35$ is “far” from the center of the excitation.

remains finite in the thermodynamic limit. This mean-field state has been argued⁶ to be unstable at finite N , due to strong gauge fluctuations. The finite N ground state is believed to spontaneously break some lattice symmetry to form a valence-bond crystal (VBC). In fact, the mean-field energy landscape is very different from the one observed in the magnetic phase. The first local minima and saddle points are listed in Table II.

We observed a high density of local minima and saddle points, with very small Hessian eigenvalues. This high density of excited saddle points reflects the presence of some strong gauge fluctuations at (large but) finite N . We note that several such saddle points display modulations of the bond amplitudes $|A|$ that have the same symmetries as the VBC previously considered for square lattice antiferromagnets. The first excitations (line a in Table II) shows a one-dimensional modulation, which is predicted to occur at finite N when $\kappa = 2 \bmod 4$.⁶ And among the highly symmetric solutions we also note a plaquette VBC ($E = -1.82534862050$) (see Fig. 6). This state does, however, not correspond to a simple VBC since it is a complex/chiral solution with nontrivial (different from 0 or π) fluxes on all the square plaquettes. See also Fig. 7 for another VBC-like state. According to the analysis of Read and Sachdev, nonperturbative gauge fluctuations (proliferation of hedgehogs point-like instantons) are responsible for the lattice symmetry breaking at finite N , leading to a modulation of $|A|$, which is exponentially small in N . The mechanism is somewhat different here since we observe VBC-like low-energy saddle points although gauge fluctuations are completely absent (all the A_{ij} are frozen in the SBMFT).

B. Triangular lattice

1. Hessian of the ground state

On the triangular lattice, we find that the lowest energy state corresponds to the (spatially uniform) solution studied by Sachdev⁹ (0-flux state¹⁵) and leads to magnetic long-range order ($\sqrt{3} \times \sqrt{3}$) for $\kappa > 0.34$, and a gapped and deconfined \mathbb{Z}_2 liquid for $\kappa \lesssim 0.34$. As usual, these two phases can be distinguished by the spinon gap: it drops to zero when increasing the system size in the magnetic phase and stays finite in the liquid phase (see Fig. 8).

The Hessian has a large lowest eigenvalue, which indicates the stability of this mean-field state with respect to $1/N$

TABLE II. Low-energy saddle points for a square lattice cluster with 36 sites, $\kappa = 0.1$. Solutions a and b are displayed in Fig. 6, and solution c is shown in Fig. 7.

E	Δ	H	d	N_λ	\min_λ	\max_λ	$N_{ A }$	$\min_{ A }$	$\min_{ A }$
-1.83492169860	0.40562447718	0.0514862091	1	1	-0.62322660824	-0.62322660824	1	0.11828994799	0.11828994799
-1.83349695884 ^a	0.43766690295	-0.0513757991	2	1	-0.62174106995	-0.62174106995	2	0.11707639293	0.11940834877
-1.83265972180	0.42301616405	3.3891521814e-05	36	6	-0.62283957972	-0.61901747505	12	0.11749362973	0.11895083747
-1.83265969367	0.42301757051	-3.3879532685e-05	72	12	-0.62289751868	-0.61872552844	25	0.11742978176	0.11900687718
-1.83265966553	0.42301846049	-3.3877477372e-05	36	10	-0.62295399258	-0.61842513968	12	0.11745616476	0.11898150831
-1.83162471056	0.41456789451	-0.2513880759	36	6	-0.62576828556	-0.60318829800	12	0.10370572327	0.13006171701
-1.83121683711	0.41375814481	-0.2872095650	72	12	-0.63567288324	-0.58931901135	25	0.03077944153	0.13945180759
-1.83088353771	0.43032855876	-0.2737625727	72	9	-0.62660943591	-0.60282776054	24	0.10017310034	0.13081740450
-1.83047599540	0.42976957584	-0.3191268237	72	12	-0.63670770779	-0.58921985280	25	0.01544819043	0.13979752631
-1.83036799495	0.43107796748	-0.3414892108	72	12	-0.63601360482	-0.58745590945	25	0.00522910878	0.14104278833
-1.83004203619	0.43897814318	-0.2774384716	36	6	-0.62530891168	-0.60252710044	12	0.10277137746	0.13077306110
-1.82976553423 ^c	0.44236450064	0.0004197766	9	3	-0.62142264885	-0.61823831215	4	0.11796026878	0.11822830533
...									
-1.82534862050 ^b	0.45598298556	0.0049547827	4	1	-0.61651000360	-0.61651000360	2	0.11510636037	0.12084117665

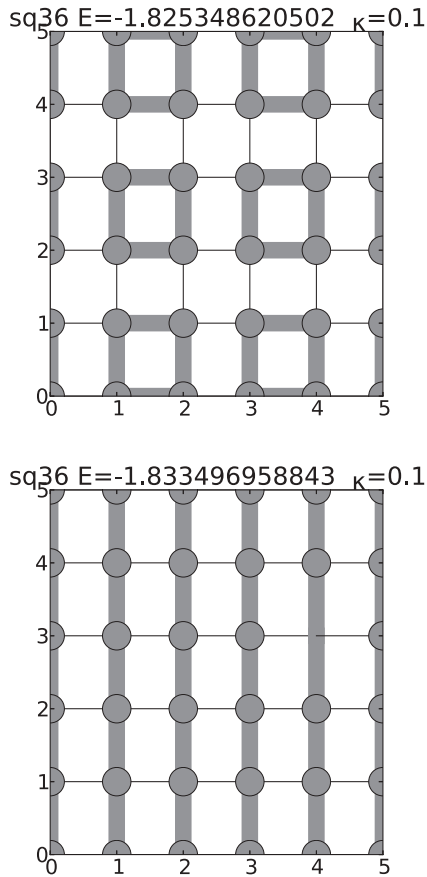


FIG. 6. Two low-energy mean-field solutions on a square lattice with 36 sites and $\kappa = 0.1$. $|A|$ takes only two values and the bonds with the stronger $|A|$ are indicated by fat grey lines (for values, see Tab. II). All the sites are equivalent and the chemical potential is uniform in both cases.

fluctuations. The evolution of this lowest eigenvalue is plotted in Fig. 8. It slightly decreases with the system size (comparing 36 and 144 sites), but is certainly finite in the thermodynamic limit. Contrary to the square lattice situation, one does not

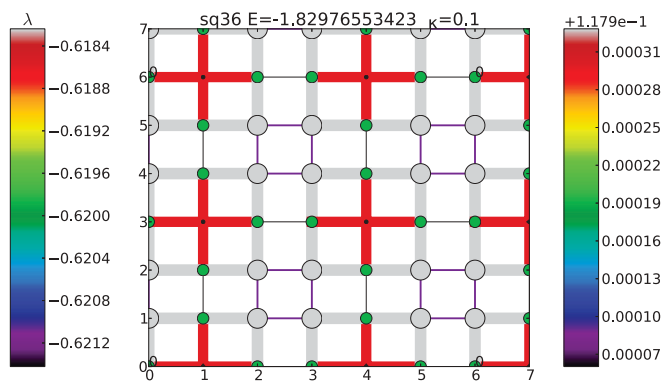


FIG. 7. (Color online) A low-energy mean-field solution on a square lattice with 36 sites and $\kappa = 0.1$. The modulus of the bond parameters is indicated—the right color scale shows deviations from the minimum value. The left color scale indicates the chemical potentials (dot on each site). This solution shows modulations with the symmetries of a 3 unit cell VBC.

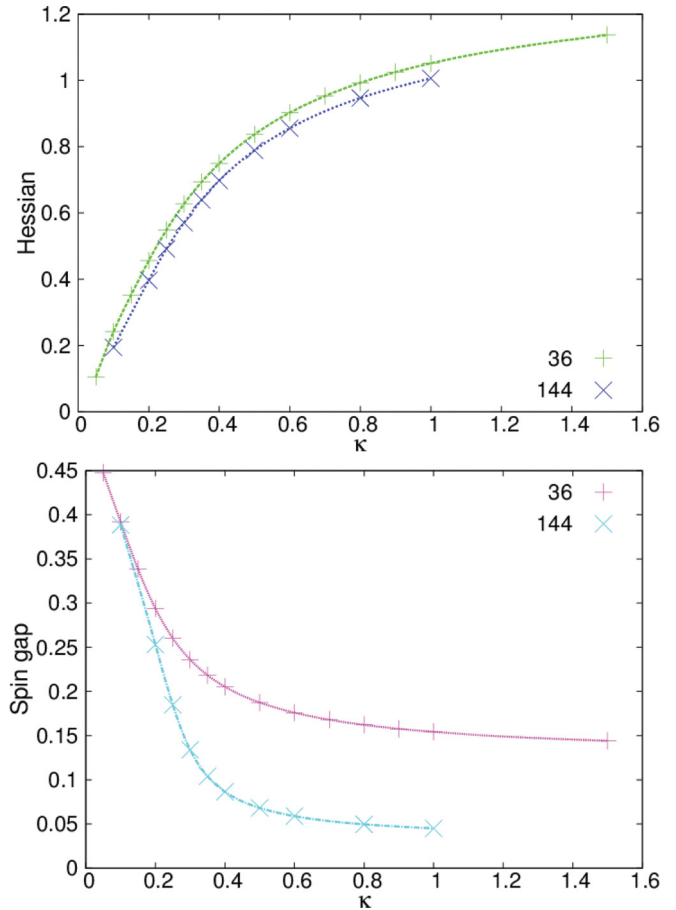


FIG. 8. (Color online) (Top) Smallest eigenvalue of the Hessian for the ground state on 36-site and 144-site triangular clusters. (Bottom) Spin gap. In the thermodynamic limit, this state is associated to magnetic long-range order (vanishing spin gap) for $\kappa \gtrsim 0.34$.⁹

detect any dramatic change of behavior between the gapped phase and the magnetic one.

In fact, since the lattice is no bipartite, the IGG of the uniform mean-field state is discrete (\mathbb{Z}_2) and we do not expect any gapless modes associated to *small* perturbations $A_{ij} = A_{ij}^0 + dA_{ij}$ with $|dA_{ij}| \ll 1$. Still, important \mathbb{Z}_2 (gapped) gauge excitations are expected in the spin liquid phase, and they will be discussed in Sec. IV B3.

The lowest eigenvector of the Hessian is represented in Fig. 9 for $\kappa = 0.1$. As in all the cases we looked at, it correspond to a *phase* fluctuation of the bond variables. The associated flux modulations for all diamond loops are shown in the bottom panel of the figure (note that the sign of each flux is somehow arbitrary since it depends on the choice of an origin of the loop). This mode represent the lowest energy $U(1)$ gauge excitation. It is gapped since $U(1)$ is *not* the low-energy gauge group (IGG) of this mean-field state.

2. Excited mean-field solutions

In Table III, we list these first mean-field states obtained for $\kappa = 1$ in a 36-site sample. As for the square lattice in its magnetic phase, we only find saddle points and no local minima among the first states. The first excited saddle point is at an energy 0.94927 above the ground state and this gap

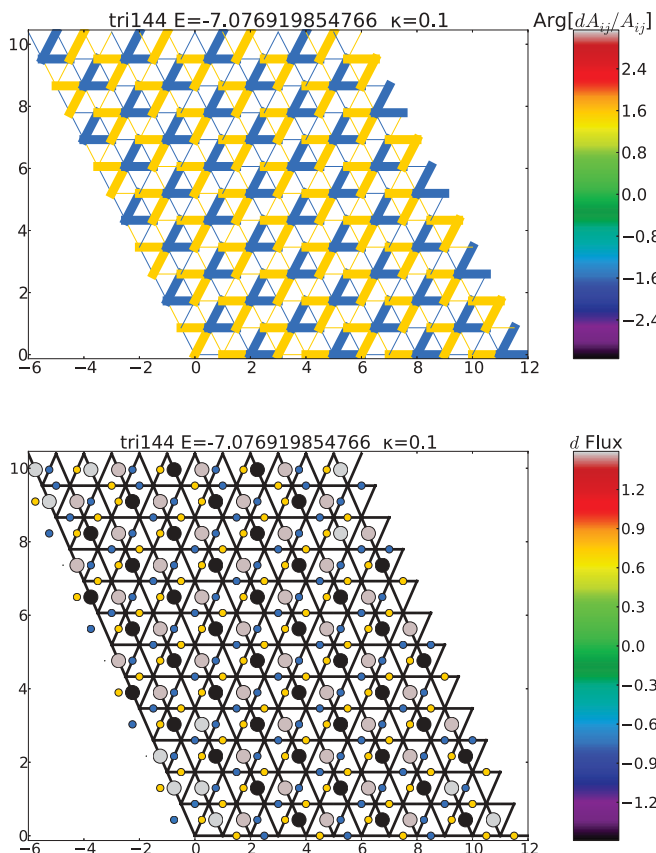


FIG. 9. (Color online) Hessian eigenvector dA/A corresponding to the smallest (degenerate) eigenvalue (0.1943) for a 144-site triangular lattice with $\kappa = 0.1$ (uniform ground state). The complex argument of dA/A take only two values: $\pm\pi/2$ (blue and yellow), indicating that dA is a (gapped $U(1)$) gauge excitation. (Bottom) Infinitesimal flux variation dF associated to the gauge mode above. For each diamond, the magnitude of the flux variation is indicated by the radius of the dot in its center (see color scale for the sign).

is very likely finite in the thermodynamic limit. This excited state has the spatial structure of a localized excitations (see Fig. 10) that resembles that of the square lattice. Finally, we note that contrary to the square lattice case, the lowest energy

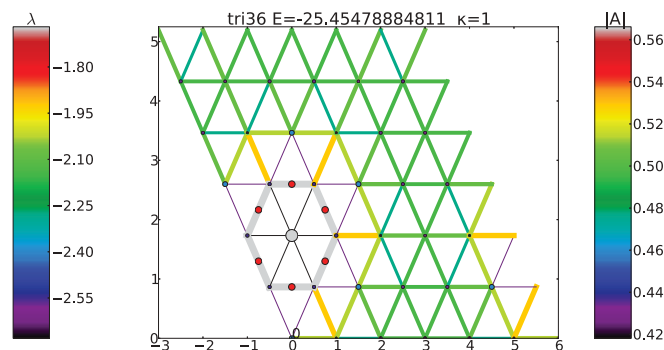


FIG. 10. (Color online) First excited state on a triangular cluster with 36 sites and $\kappa = 1$. The bond moduli are invariant by lattice rotations about the site largest chemical potential (grey circle). The flux vanish on all diamonds except for the six diamonds which diagonal bond is marked by a red dot. The later have flux π . Notice the similarity with Fig. 4.

states of Table III have real bond amplitudes (more precisely: can be made real with an appropriate gauge choice), indicating the coplanar nature of their spin-spin correlations.

For small enough κ , the SBMFT describes a gapped spin liquid of \mathbb{Z}_2 type.^{9,15} Table IV gives the first saddle points obtained at $\kappa = 0.1$. The ground state is uniform and all the rhombi have a vanishing flux, as expected. The first excited saddle point has slight modulations ($\sim 6 \times 10^{-4}$) of the bond amplitudes (see Fig. 11). This state also has vanishing fluxes on all the rhombi, but it differs from the ground state by the presence of an additional flux π along some long loop winding around the torus (three possible choices). These three states become homogeneous in the thermodynamic limit and degenerate with the ground state. With the ground state they form the fourfold topological degeneracy of the \mathbb{Z}_2 liquid on a torus.^{3,35} These states were found by the optimization algorithm starting from random initial conditions, and not “forced” by hand. We are thus confident that the method is able to find the low-energy solutions in a systematic way on small clusters at least up to a few tens of sites and bonds.

Above the four topological ground states we observe many saddle points which do not show any simple/regular spatial

TABLE III. Energy minimum and low-energy saddle points for a triangular lattice cluster with 36 sites and $\kappa = 1$. Notice that the ground state is very stable (large Hessian gap: 1.051) and that all the other saddle points are unstable (negative Hessian eigenvalue). The gap $-25.454 + 26.404 = 0.949$ is quite large. The ground state ($E = -26.40405992819$) is a solution with vanishing flux on all the diamonds and three-sublattice long-range spin-spin correlations (the critical value for magnetic long-range order is $\kappa = 0.34$).⁹ The bond strength of the first excited state are displayed in Fig. 10.

E	Δ	H	d	N_λ	\min_λ	\max_λ	$N_{ \lambda }$	$\min_{ \lambda }$	$\min_{ \lambda }$	
-26.40405992819	0.15424645309	1.0517831524	1	1	-2.58830049633	-2.58830049633	1	0.49723336391	0.49723336391	R
-25.45478884810	0.14039937369	-2.3583827803	36	7	-2.68083518864	-1.66967911414	12	0.41812686812	0.56615895080	R
-24.89782095003	0.13788292075	-2.1218542408	108	12	-2.66775663053	-1.86004294873	31	0.25950830810	0.56907182479	R
-24.88367410179	0.11975325026	-2.3419680753	432	36	-2.76307967976	-1.75626091358	108	0.13936678359	0.57983094362	R
-24.88248919944	0.14303067790	-2.3536310845	216	18	-2.72365738218	-1.77512884614	56	0.18149763138	0.57925175603	R
-24.85225639276	0.05506495561	-2.6494385700	216	21	-2.87033693396	-1.82953713470	57	0.05089520618	0.56602789699	R
-24.54012950533	0.07534371832	-2.7179265074	216	18	-2.83154574151	-1.61720470431	56	0.25139432620	0.57460696668	R
-24.52557412388	0.06458137688	-2.4327487996	216	18	-2.82124110423	-1.87789249232	56	0.09674702612	0.56912072760	R
-24.51689402152	0.10842201321	-2.4288970581	72	10	-2.79081268614	-1.66076773241	21	0.35681606435	0.56617071630	R
-24.42913380032	0.13143243020	-2.5993027532	54	8	-2.66560684707	-1.62001869447	17	0.38239562932	0.56552771557	R
-24.38386557808	0.12833408469	-2.0204356396	108	13	-2.73034611703	-1.88206681620	30	0.25362349993	0.56892183451	R
-24.36651624089	0.11045933281	-2.2168211792	432	36	-2.76253254084	-1.77578363386	108	0.10590160533	0.58136368633	R

TABLE IV. Low-energy saddle points for a triangular lattice cluster with 36 sites and $\kappa = 0.1$. The ground state and the first excited saddle point ($E = -1.76857445623$, threefold degenerate) form the fourfold topological degeneracy.^{3,35} The other saddle points listed here are chiral(complex), except for the last line, which corresponds to a pair of visons (see Sec. IV B3 and Fig. 12).

E	Δ	H	d	N_λ	\min_λ	\max_λ	$N_{ A }$	$\min_{ A }$	$\max_{ A }$	
-1.77115513853	0.39183413870	0.2418792448	1	1	-0.63927958247	-0.63927958247	1	0.09721004221	0.09721004221	R
-1.76857445623	0.43969994315	0.1404951036	3	1	-0.63620536809	-0.63620536809	2	0.09694182615	0.09756074413	R
-1.76558449027	0.40008559551	-0.0136673394	108	13	-0.64036695527	-0.61163933625	30	0.08631046645	0.10220320383	C
-1.76556438644	0.39881698544	-0.0662494156	216	21	-0.64094448900	-0.60807754792	57	0.07142251452	0.11045947514	C
-1.76519815707	0.40323866935	-0.0476017475	216	21	-0.64101212209	-0.62149883058	57	0.08166138572	0.10941122095	C
-1.76517640350	0.40348584568	-0.0574617718	432	36	-0.64242077150	-0.62028199544	108	0.08102625728	0.11240116020	C
-1.76512811482	0.40255745524	-0.0675887556	216	21	-0.64418307267	-0.62192577975	57	0.07214207918	0.11553853523	C
-1.76498033616	0.40426965800	-0.0822323880	216	18	-0.64027903292	-0.62235496321	56	0.07818420245	0.11549233664	C
-1.76494386569	0.40647240030	-0.0077675537	108	12	-0.64031335557	-0.61976563929	31	0.08656330909	0.10201782841	C
-1.76490270376	0.41103320490	0.0552851450	216	18	-0.64030870204	-0.62463756694	56	0.08904499619	0.10413653140	C
-1.76486322625	0.40885376933	-0.0517770911	432	36	-0.64144886953	-0.62152076605	108	0.08370457723	0.10627245220	C
-1.76481070231	0.40714839383	-0.0588744760	216	18	-0.64059451058	-0.62076171059	56	0.08285231897	0.10673538608	C
...										
-1.76267094982	0.41119320956	-0.2136294440	108	12	-0.64647502600	-0.60434357136	31	0.07784772351	0.11384461169	R

pattern (high number of inequivalent sites and bonds). These states have energies significantly below the first vison-pair state we have found (last line in Table IV and Fig. 12). Due to the presence of complex fluxes (not 0 or π), these states do not have a simple interpretation in terms of the \mathbb{Z}_2 gauge field. The presence of these additional degrees of freedom is somewhat intriguing since the low-energy description of such a short-ranged RVB phase is expected to be \mathbb{Z}_2 , a gauge theory coupled to gapped spinons.

3. Visons

A \mathbb{Z}_2 liquid possesses nonmagnetic excitations named *visons*, which correspond to π -flux quanta of the effective Ising gauge theory.^{6,35} In a finite system (without boundaries), the number of vison is necessarily even, and a trial vison-pair state can be constructed as follows. One starts from the uniform mean-field ground state and one reverses the sign of the bond parameters A_{ij} for all the bonds ij crossing a cut extending from the a first plaquette to a second one. The gauge flux

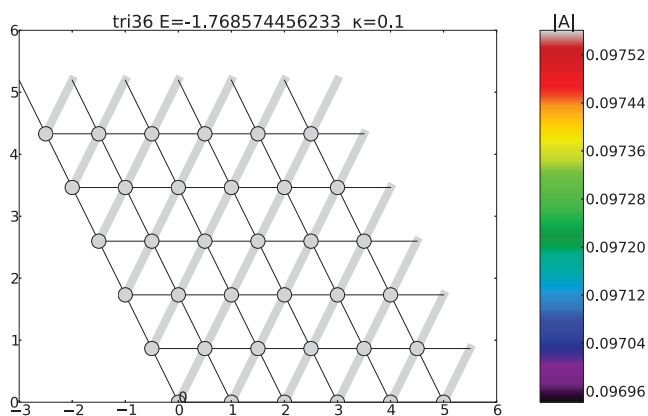


FIG. 11. (Color online) First excitation on a triangular cluster with 36 sites and $\kappa = 0.1$. This state is threefold degenerate. With the ground state, it forms the fourfold topological degeneracy expected for a \mathbb{Z}_2 liquid on a torus. Notice (scale on the right) that the difference between the largest $|A_{ij}|$ and the smallest one is only $\sim 6 \cdot 10^{-4}$ and should vanish in the thermodynamic limit.

is then concentrated in the immediate vicinity of these two plaquettes, which correspond to the vison core positions. Any gauge-invariant operator far from the vison cores is unaffected by this modification.

Due to the presence of flux π for each loop encircling a vison core, such a trial state is in general not self-consistent ($\langle \hat{A}_{ij} \rangle \neq A_{ij}$ and $\langle \hat{n}_i \rangle \neq \kappa$). To obtain a self-consistent state (saddle point), the bond moduli as well as the chemical potentials should be re-adjusted in the vicinity of the vison cores. We obtain numerically such self-consistent vison-pair

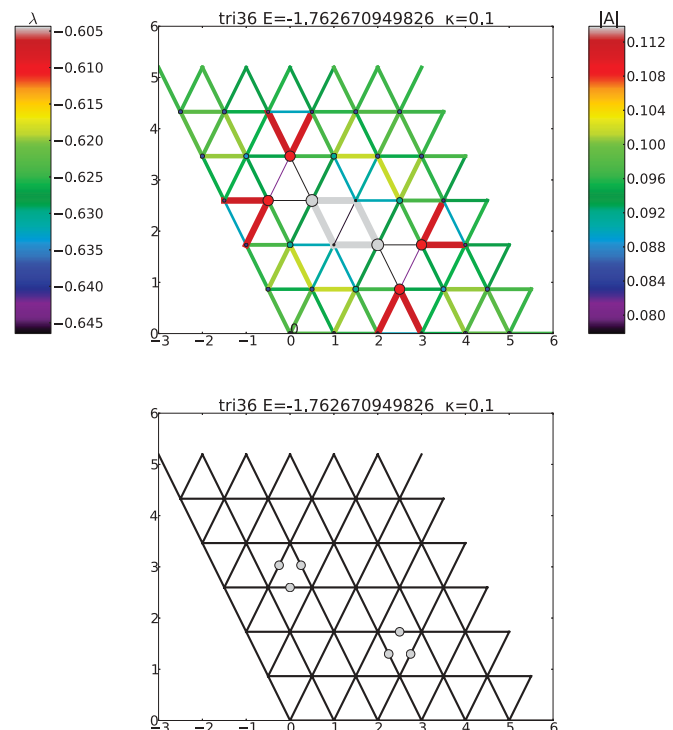


FIG. 12. (Color online) (Top) Modulus $|A|$ and chemical potential for a saddle point with two visons at distance $d = 5\sqrt{3}/3$, (6×6 triangular lattice, $\kappa = 0.2$). (Bottom) Flux vanishes on all diamonds except those with the diagonal tagged with a grey circle. The visons are localized on the triangles with three such circles.

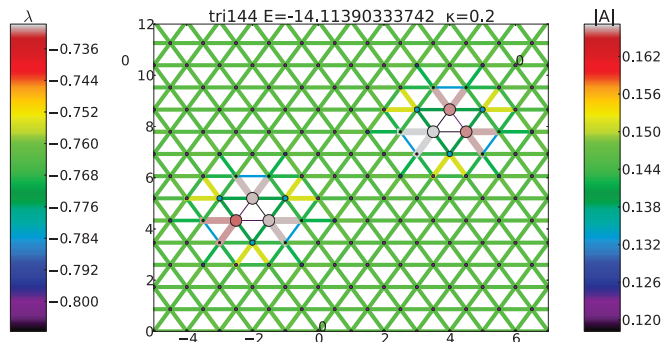


FIG. 13. (Color online) Modulus $|A|$ and chemical potential for a saddle point with two visons at distance $d = 4\sqrt{3}$, (12×12 triangular lattice, $\kappa = 0.2$). A string of reversed A_{ij} (not shown) goes from the first vison core to the second.

states by looking at the nearest saddle point in the vicinity of the trial state (second stage of the algorithm described in Sec. III B). These gives access to some energetics of the visons, and to their energy as a function distance in particular.

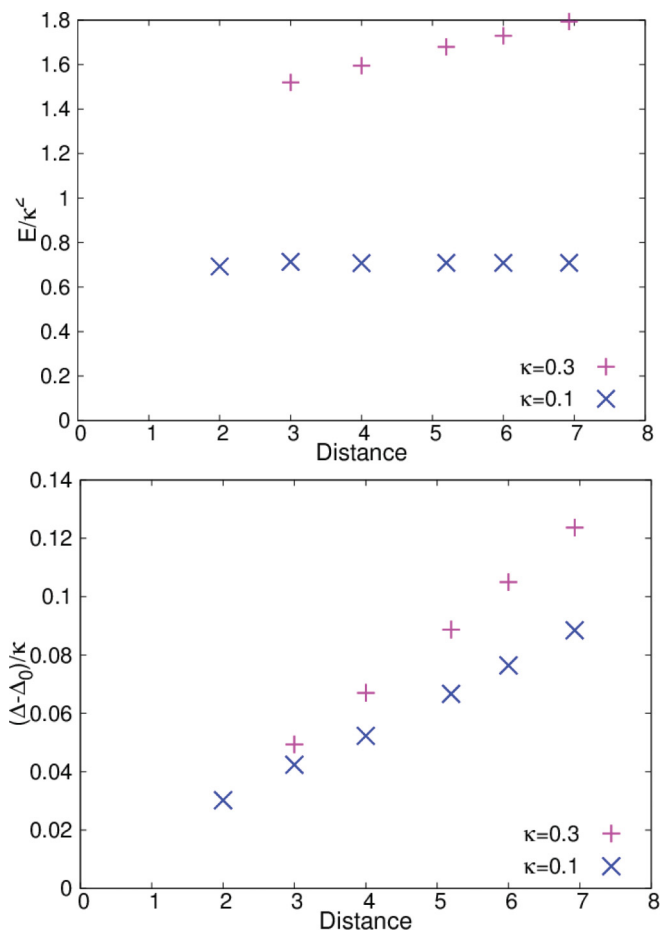


FIG. 14. (Color online) (Top) Energy cost of a pair of visons as a function of distance in a 144-site triangular cluster. (Bottom) Difference between the spinon gap Δ in presence of the two visons, and the gap Δ_0 in the absence of visons. This difference has been scaled by κ to compare $\kappa = 0.1$ and $\kappa = 0.3$. Since $\Delta > \Delta_0$, there is some *repulsion* between a spinon and a vison pair.

Typical vison-pair solutions are displayed in Figs. 12 and 13. The modulation of $|A|$ in the vicinity of each vison is clearly visible, as well as the higher (less negative) chemical potentials in the core regions. In this case ($\kappa = 0.2$), the vison core radius is of the order of two lattice spacings. These excited states are, however, not local minima, but saddle points. In all the cases considered here (vison distance from 2 to $4\sqrt{3}$), we find four negative Hessian eigenvalues, with a rather weak dependence on the vison separation.

A calculation of the bond modulations in a vison mean-field state was recently carried out by Huh, Punk, and Sachdev³⁶ using an effective model valid in the limit of large spinon gap. Their result indicates that $|A_{ij}|$ decreases on all the bonds close to the vison core. In our calculation, it appears that the some moduli are indeed depressed, but some are also enhanced (red bonds in Fig. 12 and grey bonds in Fig. 13).

Some aspects of the visons energetics are summarized in Fig. 14. In the large- N framework, these energies should be multiplied by a factor N . It can be checked that their mutual interaction is very weak, since the total energy hardly depends

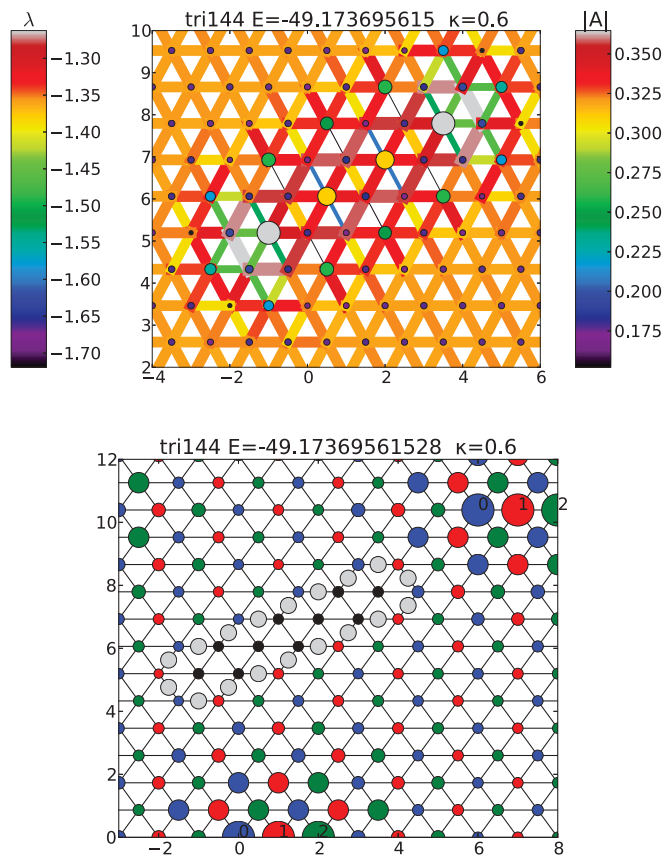


FIG. 15. (Color online) Highly excited solution on the triangular lattice (144 sites) with $\kappa = 0.6$ (ordered phase). (Top) Bond amplitudes. (Bottom) Spin-spin correlations and fluxes. If $\langle S_0 \cdot S_i \rangle$ is positive while $\langle S_1 \cdot S_i \rangle$ and $\langle S_2 \cdot S_i \rangle$ are negative, the site i is said to belong to the “0” sublattice (blue circles). Likewise, the site which are positively correlated with site 1 (respectively 2) are marked in red (respectively green). The other sites are marked in black and the radius of the circle is proportional to the maximum of $|\langle S_0 \cdot S_i \rangle|$, $|\langle S_1 \cdot S_i \rangle|$ and $|\langle S_2 \cdot S_i \rangle|$. The diamonds have vanishing flux except for those marked by a grey circle, which have a flux π (see text).

on the distance, as expected in a gapped \mathbb{Z}_2 liquid phase. These calculations also provide some information about the spinon-vison interactions. This question is important since vison-spinon bound states have fermionic mutual statistics.³⁵ It appears, however, that the spinon gap Δ is slightly *higher* in presence of a vison pair than in the ground state (Δ_0). This indicates some vison-spinon repulsion and makes unlikely the existence of a bound-state between these two excitations.

We investigated the effect of inserting two π fluxes far apart in the magnetic phase of the model. Since the system is magnetically ordered, visons are no longer low-energy excitations. Starting from a vison-pair trial state we look for the nearest self-consistent mean-field state. A typical result is shown in Fig. 15, where the initial state was chosen to have two localized visons at the same locations as in Fig. 13. At the end of the numerical optimization (stage 2 only), it appears the algorithm has converged to a (unstable) saddle points where some additional pairs diamonds with flux π are present. These additional fluxes form an elongated ring enclosing the two initial vison cores. Contrary to the vison-pair states in the liquid phase, the spin-spin correlations are strongly modified all the way inside the ring (bottom panel of Fig. 15). Indeed, the three sublattice is destroyed, although the spin-spin correlations remain large (black circle radii). This state appears to be similar to a classical vortex/antivortex pair.

V. SUMMARY AND CONCLUSIONS

We have developed a numerical method to explore the low-energy SBMFT solutions on finite clusters up to one hundred bonds, without any assumption on the symmetries of the solutions. The algorithm is able to determine the global energy minimum, the spectrum of its Hessian matrix, as well as excited saddle points. The high numerical accuracy allows to resolve saddle points with small energy differences and very weak spatial modulations. The Bogoliubov spectrum of *spinons* excitations has already been discussed at length in the literature on SBMFT. In this work, we instead focused on the *nonmagnetic* excitations associated to small (quadratic) bond fluctuations in the vicinity of the ground state, or those that correspond to excited saddle points.

At low κ , the SBMFT describes spin liquids with gapped spinons. In the square lattice case our calculations confirmed that some low-energy nonmagnetic excitations are associated to gauge degrees of freedom. These excitations are gapless,

and linearly dispersing U(1) “photons”. They are associated to the first eigenvalues of the Hessian describing small amplitude phase fluctuations in the vicinity of the ground state. As expected, we observe that these photons get gapped when entering the magnetically ordered phase, due to spinons condensation. On the triangular lattice, we found saddle points corresponding to pairs of \mathbb{Z}_2 vortices (visons). We presented some results concerning the energetics of these visons (gap and weak mutual attraction).

In addition to these excitations, which are qualitatively well understood, the SBMFT energy landscape revealed in all cases a large number of low-energy excited saddle points, which do not appear to correspond to some intuitively simple excitation. For instance, on the triangular lattice, the presence of low-energy saddle points with complex/chiral fluxes do not have a simple explanation in terms of the \mathbb{Z}_2 gauge degrees of freedom that are expected to describe the low-energy physics of a short-range RVB spin liquid. This surprising observation clearly deserves further investigations. Can they be related to some real *spin* excitations or are they specific to the $N = \infty$ limit? Can they provide some information about the finite N fluctuations?

In the magnetic phases of the square and triangular lattice models, the first excited saddle point turn out to be a pointlike object, with some spin “texture” localized around some core. This texture appears to be planar in the triangular case and nonplanar in the square lattice case, but here also the precise connection with spin excitations of an $SU(2)$ model is not obvious. The present study is probably just a first descriptive step toward a better understanding of this large- N limit.

We finally mention that, on the kagome lattice, this approach also reveals a complex landscape with tiny energy scales, and some unexpected symmetry breaking in the (mean-field) ground state of small clusters. Work is in progress to determine the actual ground state symmetry on larger clusters (108 sites in particular), where none of the two well-studied states ($\sqrt{3} \times \sqrt{3}$ and $q = 0$) is the the lowest-energy state for $\kappa = 1$.³¹

ACKNOWLEDGMENTS

I wish to thank Laura Messio, Claire Lhuillier, Vincent Pasquier, Roderich Moessner, and Shivaji Sondhi for useful discussions. Part of the calculations were performed on the computers *titane* and *airain* at the *Centre de Calcul Recherche et Technologie* of the CEA.

¹L. Balents, *Nature (London)* **464**, 199 (2010).

²I. Affleck, *Phys. Rev. Lett.* **54**, 966 (1985).

³N. Read and S. Sachdev, *Phys. Rev. Lett.* **66**, 1773 (1991).

⁴D. Rokhsar, *Phys. Rev. B* **42**, 2526 (1990).

⁵A. E. Trumper, L. O. Manuel, C. J. Gazza, and H. A. Ceccatto, *Phys. Rev. Lett.* **78**, 2216 (1997).

⁶N. Read and S. Sachdev, *Phys. Rev. Lett.* **62**, 1694 (1989).

⁷D. Arovas and A. Auerbach, *Phys. Rev. B* **38**, 316 (1988).

⁸F. Mila, D. Poilblanc, and C. Bruder, *Phys. Rev. B* **43**, 7891 (1991).

⁹S. Sachdev, *Phys. Rev. B* **45**, 12377 (1992).

¹⁰C. J. Gazza and H. A. Ceccatto, *J. Phys.: Condens. Matter* **5**, L135 (1993).

¹¹C. H. Chung, J. B. Marston, and R. H. McKenzie, *J. Phys.: Condens. Matter* **13**, 5159 (2001).

¹²A. Mezio, C. N. Sposetti, L. O. Manuel, and A. E. Trumper, *Europhys. Lett.* **94**, 47001 (2011).

¹³A. Mattsson, P. Fröjdh and T. Einarsson, *Phys. Rev. B* **49**, 3997 (1994).

- ¹⁴F. Wang, *Phys. Rev. B* **82**, 024419 (2010).
- ¹⁵F. Wang and A. Vishwanath, *Phys. Rev. B* **74**, 174423 (2006).
- ¹⁶Tiamhock Tay and O. I. Motrunich, *Phys. Rev. B* **84**, 193102 (2011).
- ¹⁷L. Messio, B. Bernu, and C. Lhuillier, *Phys. Rev. Lett.* **108**, 207204 (2012).
- ¹⁸B. Fåk *et al.*, *Phys. Rev. Lett.* **109**, 037208 (2012).
- ¹⁹M. Albrecht and F. Mila, *Europhys. Lett.* **34**, 145 (1996).
- ²⁰C. H. Chung, J. B. Marston, and S. Sachdev, *Phys. Rev. B* **64**, 134407 (2001).
- ²¹M. Albrecht and F. Mila, *Phys. Rev. B* **53**, R2945 (1996).
- ²²M. Hermele, V. Gurarie, and A. M. Rey, *Phys. Rev. Lett.* **103**, 135301 (2009); M. Hermele and V. Gurarie, *Phys. Rev. B* **84**, 174441 (2011).
- ²³A. Auerbach, *Interacting Electrons and Quantum Magnetism* (Springer-Verlag, Berlin, 1994).
- ²⁴G. Misguich, [arXiv:0809.2257](https://arxiv.org/abs/0809.2257).
- ²⁵H. A. Ceccatto, C. J. Gazza, and A. E. Trumper, *Phys. Rev. B* **47**, 12329 (1993).
- ²⁶R. Flint and P. Coleman, *Phys. Rev. B* **79**, 014424 (2009).
- ²⁷This mean-field Hamiltonian is the same as that obtained in the $N \rightarrow \infty$ limit of the $\text{Sp}(N)$ generalization of the Heisenberg model.³
- ²⁸J. H. P. Colpa, *Physica A* **93**, 327 (1978).
- ²⁹From Eq. (12), we have $\partial E/\partial\lambda = \kappa - \langle \hat{n}_i \rangle$ and $\partial^2 E/\partial\lambda^2 = -\partial \langle \hat{n}_i \rangle/\partial\lambda$. Using first-order perturbation theory, the last expression can be shown to be negative.
- ³⁰O. Tchernyshyov, R. Moessner, and S. L. Sondhi, *Europhys. Lett.* **73**, 278 (2006).
- ³¹G. Misguich (unpublished).
- ³²M. I. A. Lourakis, levmar: Levenberg-Marquardt nonlinear least squares algorithms in C/C++, <http://www.ics.forth.gr/~lourakis/levmar/>.
- ³³L. Messio, Ph.D. thesis, Universite P. et M. Curie, 2010.
- ³⁴X.-G. Wen, *Phys. Rev. B* **65**, 165113 (2002).
- ³⁵N. Read and B. Chakraborty, *Phys. Rev. B* **40**, 7133 (1989).
- ³⁶Y. Huh, M. Punk, and S. Sachdev, *Phys. Rev. B* **84**, 094419 (2011).